Heliyon 9 (2023) e15678

Contents lists available at ScienceDirect

Heliyon

journal homepage: www.cell.com/heliyon

Research article

Efficiency of Ag_3PO_4/TiO_2 as a heterogeneous catalyst under solar and visible light for humic acid removal from aqueous solution

Roya Morovati [a,b], Saeed Rajabi [a,b], Mohammad Taghi Ghaneian [c], Mansooreh Dehghani [a,*]

[a] Department of Environmental Health Engineering, School of Health, Shiraz University of Medical Sciences, Shiraz, Iran
[b] Student Research Committee, School of Health, Shiraz University of Medical Sciences, Shiraz, Iran
[c] Environmental Science and Technology Research Center, Department of Environmental Health Engineering, School of Health, Shahid Sadoughi University of Medical Sciences, Yazd, Iran

ARTICLE INFO

Keywords:
Humic acid
Heterogeneous catalyst
Photocatalytic
Solar light
Visible light

ABSTRACT

Nowadays, the presence of humic acid (HA) in water sources is highly regarded due to the production of extremely harmful byproducts such as trihalomethanes. In this study, the effectiveness of an Ag_3PO_4/TiO_2 catalyst produced by in situ precipitation as a heterogeneous catalyst for the degradation of humic acid in the existence of visible and solar light was evaluated. The Ag_3PO_4/TiO_2 catalyst's structure was characterized using X-ray powder diffraction (XRD), scanning electron microscopy (SEM), and energy dispersive spectroscopy (EDS), after which the catalyst dosage, HA concentration, and pH parameters were adjusted. After a 20-min reaction, the highest HA degradation of 88.2% and 85.9% in presence of solar light and visible light were attained at the ideal operating conditions of 0.2 g/L catalyst, 5 mg/L HA, and pH 3, respectively. It was discovered that, based on kinetic models, the degradation of HA matched both Langmuir-Hinshelwood and *pseudo*-first-order kinetics at concentrations of 5 to 30 mg/L ($R^2 > 0.8$). The Langmuir-Hinshelwood model had surface reaction rate constants (K_c) of 0.729 mg/L.min and adsorption equilibrium constants ($K_{L\text{-}H}$) of 0.036 L/mg. Eventually, a real-water investigation into the process' effectiveness revealed that, under ideal circumstances, the catalyst had a reasonable HA removal efficiency of 56%.

1. Introduction

One of the current environmental issues is the existence of organic contaminants in water supplies, including humic acids (HA). One of the primary components of natural organic matter (NOM) is humic acid, a non-uniform macromolecular polymer [1,2]. In both surface and groundwater, HA is a complicated molecule that is frequently present. Humic acid concentrations in drinking water have been measured to be between 2 and 15 mg/L [3,4].

Humic acids include organic functional groups including hydroxyl, carboxyl, carbonyl, methoxy, and quinone groups that can interact with organic and inorganic contaminants in water through mechanisms like absorption, ion exchange, and chelation, resulting in a decline in water quality [5–7]. HA can dissolve in water in very acidic circumstances, whereas fulvic acid is entirely soluble in

* Corresponding author.
E-mail addresses: r_morovati@sums.ac.ir (R. Morovati), Saeedrajabi@sums.ac.ir (S. Rajabi), mtghaneian@ssu.ac.ir (M.T. Ghaneian), Mdehghany@sums.ac.ir (M. Dehghani).

https://doi.org/10.1016/j.heliyon.2023.e15678
Received 3 November 2022; Received in revised form 17 April 2023; Accepted 18 April 2023
Available online 22 April 2023

water [6,8]. As a result, it is crucial to remove HA from water sources since it serves as a precursor to disinfection byproducts, which is a challenging task. In order to remove HA from aquatic environments, several researchers have utilized a variety of techniques, including chemical coagulation [9], electrocoagulation [6], adsorption [10–14], ion exchange [15], membrane processes or membrane separation [16–18], Fenton [19,20], and photocatalysis [3,21,22]. Among these techniques, advanced oxidation processes might be considered.

Advanced oxidation processes generate free radicals with strong oxidizing activity, and as a result, organic compounds are destroyed into simple, low-danger molecules. The complete degradation of organic materials, lack of toxicity, absence of sludge generation, formation of compounds with strong oxidizing capabilities, non-corrosiveness of equipment's pieces, and simplicity of application are all benefits of this process [23,24]. Nanoparticles called nanocatalysts are utilized in advanced oxidation processes to boost effectiveness [25].

Heterogeneous catalysts provide a variety of advantages including the capacity to be reused, high stability, simplicity in separation, and cost-effectiveness. They also help the oxidation process proceed more quickly and efficiently [26,27]. Ultrasound, UV, heat, electricity, and other forms of energy are employed to activate these nanocatalysts.

In recent years, there has been a lot of interest in the photocatalytic destruction of organic molecules and environmental contaminants. Due to its unique qualities in bonding position and surface structure, chemical stability, and lack of toxicity, TiO_2 is one of the most well-known photocatalysts among other semiconductors. However, due to the high band gap distance and TiO_2's inability to use them, visible photons, which make up a considerable portion of the solar spectrum, are limited in their practical uses. In order to develop visible light photocatalysts, a variety of metal oxides, such as Ag_3PO_4 with a short band gap spacing, which provides new possibilities for photon gathering in the visible range, can be combined with TiO_2. As a novel visible light absorption semiconductor, silver orthophosphate (Ag_3PO_4), which has a dark golden hue, has frequently garnered attention [28–30].

Although various nanoparticles, including $FeNi_3$@SiO_2@TiO_2 [31], Mn_2O_3–Al_2O_3 [32], PAC-$LaFeO_3$-Cu [33], Fe_3O_4/TiO_2–N-GO [34], Ce–ZrO_2 [35], Ag/ZnO [21,36], CuO–Co_3O_4@AC [37], $FeNi_3$@SiO_2 [38] have so far been utilized as a catalyst in the degradation of humic acids.

The removal of humic acid using Ag_3PO_4/TiO_2 nanoparticles in the presence of solar light and visible light has not yet been reported. Contrary to earlier research, which employed ultraviolet light radiation for this nanoparticle. In this work, visible light and solar light were utilized to boost the effectiveness of this nanoparticle since they are more accessible, less expensive, and environmentally friendly than other methods. As a result, the goal of this study was to provide a low-cost environment in which to lower the amount of HA in water. Since spectrophotometric measurement is a convenient and effective method for detecting HA, it was also utilized in this study. The effects of the initial HA concentration, the dosage of nanoparticles, and the initial pH value on HA degradation were also investigated.

2. Materials and methods

2.1. Chemicals and instruments

Merck Company (Germany) supplied silver nitrate ($AgNO_3$). Degussa (Germany) provided the P25 titania (TiO_2), while Sigma-Aldrich provided the Na_3PO_4 for the catalyst production. Sigma-Aldrich was also used to purchase the humic acid, sodium hydroxide (NaOH), and hydrogen chloride (HCl). The pH of the solutions was adjusted with HCl and NaOH (1 *N*), and the pH was detected with a pH meter (Wegtech Mi 151 22, UK). At a maximum wavelength of 254 nm, a UV–vis spectrophotometer (Model Optima SP3000 Plus, Japan) was utilized to measure the concentration of HA. The structure of this yellow nanocomposite, which acts as a heterogeneous catalyst, was studied using XRD, SEM, and EDS tools. XRD (Bourevestnik-Dron8) was used to characterize the shape and phase of a nano-crystal catalyst, SEM (TESCAN-Vega3) was used to study the structure, morphology, and surface characteristics of the nano-catalyst on the nanoscale, and EDS (TESCAN-Vega3) was used to evaluate the component mass percentages at the nano-catalyst and BET to quantify the size of a particular area in the nanocatalyst (BELSORP MINI II). After validating the physical and chemical composition of the heterogeneous nanocatalyst, it was utilized to degrade HA in an aqueous media.

2.2. Preparation of Ag_3PO_4/TiO_2

The in situ precipitation approach developed by Yao et al. was used to synthesize silver phosphate (Ag_3PO_4) deposition onto titania (P25) [39]. In 50 mL of deionized water, 1.6 g of titania (P25 with 80% anatase and a surface area of 50 m^2/g) was disseminated and sonicated for 5 min. Following sonication, 3.05 g of $AgNO_3$ was introduced to the titania disseminated water and magnetically agitated for 10 min at 200 rpm. The sodium phosphate was distributed in 50 mL of deionized water before being dropped into the reaction mixture. For 300 min, the finished solution was magnetically agitated. The color of the mixture was then altered from white to yellow. After that, the Ag_3PO_4/TiO_2 nanocomposite was strained, rinsed with water and ethanol, and dried for 12 h at 60 °C. After preparing the heterogeneous catalyst, it was utilized in a photocatalytic process and characterization.

2.3. Batch photocatalytic experiments

The photocatalytic process was influenced by pH, catalyst dose, initial HA concentration, and contact duration, which were all investigated and modified. From a stock HA solution with a 500 mg/L concentration, HA concentrations of 5, 10, and 25 mg/L were produced. To find the optimal catalyst dose, the study examined 0.1, 0.15, 0.2, and 0.3 g/L. The experiments examined pH values of

three to eleven (3, 7, and 11), as well as contact times of 3, 5, 10, 20, 30, and 45 min. The experiment was conducted using a 250 mL aluminum-covered container with a 20-W bulb lamp for visible light, then with the same container without the aluminum cover in direct solar light. The following formulas were used to calculate the degrading efficiency of HA (Eq. (1)):

$$Removal\ Efficiency\ (\%) = \frac{C_0 - C_t}{C_0} \times 100 \quad \text{(Eq.1)}$$

Where the concentrations of HA before and after contact time are shown by C_0 and C_t (mg/L) [40].

2.4. Determine the pH_{zpc}

The pH_{zpc} was determined utilizing 50 mL of KCl 0.1 M mixture at six pHs (2, 4, 6, 8, 10, and 12) and 0.01 g of heterogeneous catalyst nanoparticles. After 24 h, set the prepared mixtures on the shaker and take the pH reading. Utilizing the formula $\Delta pH = pH_{final}\text{-}pH_{initial}$, the resulting curve was displayed as X = initial pH and Y = ΔpH. The pH_{zpc} is the X-axis point where the curve intersects [41].

3. Results and discussion

3.1. Characterization of Ag_3PO_4/TiO_2

The FESEM images of the synthesized Ag_3PO_4/TiO_2 heterogeneous catalyst were used to assess the morphology, size, and shape. FESEM images of the Ag_3PO_4/TiO_2 heterogeneous catalyst synthesized are shown in Fig. 1(a–c). The Ag_3PO_4/TiO_2 heterogeneous catalyst structure was formed into a sphere-shaped and nano-heterogeneous catalyst that was loosely aggregated, uniformly, and smoothly. The particle size of this catalyst is shown in Fig. 1c. It may be stated that the mean particle size of Ag_3PO_4/TiO_2 heterogeneous catalyst is 50–60 nm according to the particle size.

EDS analysis was used to assess the homogeneity and chemical structure of the produced Ag_3PO_4/TiO_2 heterogeneous catalyst (Fig. 2). The EDS results show that the chemical structure of Ag_3PO_4/TiO_2 heterogeneous catalyst contains 65.3% Ag, 17.7% Ti, 9.2% O, and 7.7% P, which are all within the predicted range.

XRD analysis was performed to characterize the Ag_3PO_4/TiO_2 heterogeneous catalyst's phases, structures, and crystalline constitution. Fig. 3 depicts the XRD findings. Based on the Joint Committee on Powder Diffraction Standards (JCPDS 96-591-0064), the Ag_3PO_4/TiO_2 heterogeneous catalyst crystal phase structure and XRD pattern with diffraction peaks at 2θ, except for the peak at 25.3° indexed to the (101) plane of TiO_2 (P25), additional peaks at 2θ values of 20.93° (110), 29.78° (200), 33.39° (210), 36.68° (211), 47.94° (310), 52.85° (222), 55.19° (321) indexed to Ag_3PO_4. Furthermore, the observed peak at 2θ~32.5° is attributable to the lattice distortion in the structure of the nanocatalyst caused during its synthesis. The Ag_3PO_4/TiO_2 heterogeneous catalyst crystal structure was successfully conserved, according to the findings. Its proper and high-performance synthesis was demonstrated by the findings of this nanocatalyst's characterization, which were extremely comparable and consistent to those of the nanocatalyst synthesized by Taheri et al. [24].

The Ag_3PO_4/TiO_2 adsorption/desorption isotherm and the BJH specific surface area are shown in Fig. 4. To determine the Ag_3PO_4/TiO_2 nanocatalyst's BET surface area, N_2 adsorption/desorption studies were conducted. The monolayer volume of gas adsorbed was calculated using the BET equation, which can then be used to determine the surface area of the adsorbent [42]. The total pore volume and BJH of the produced nanocatalyst ($p/p_0 = 0.990$) were calculated using the ADS/DES plot. This value was 47.138 m^2/g.

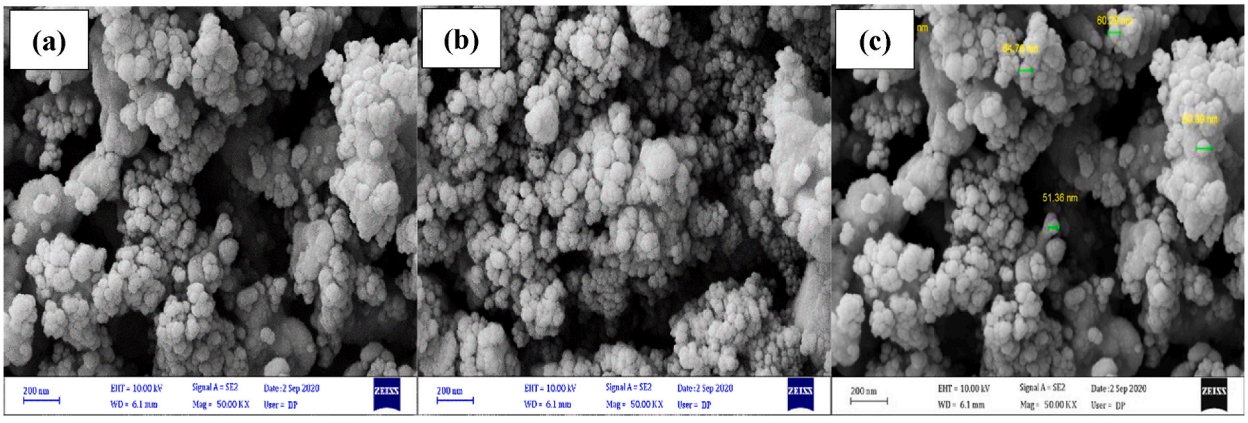

Fig. 1. SEM images (a–c) of Ag_3PO_4/TiO_2 heterogeneous catalyst.

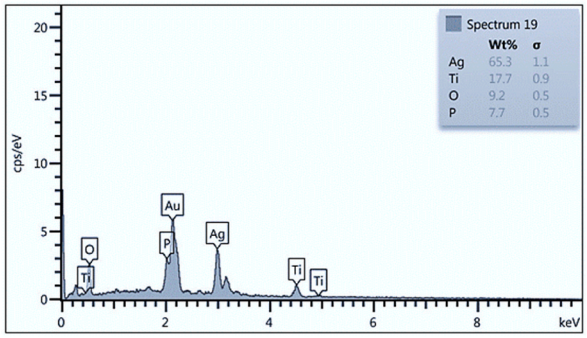

Fig. 2. EDS of Ag_3PO_4/TiO_2 heterogeneous catalyst.

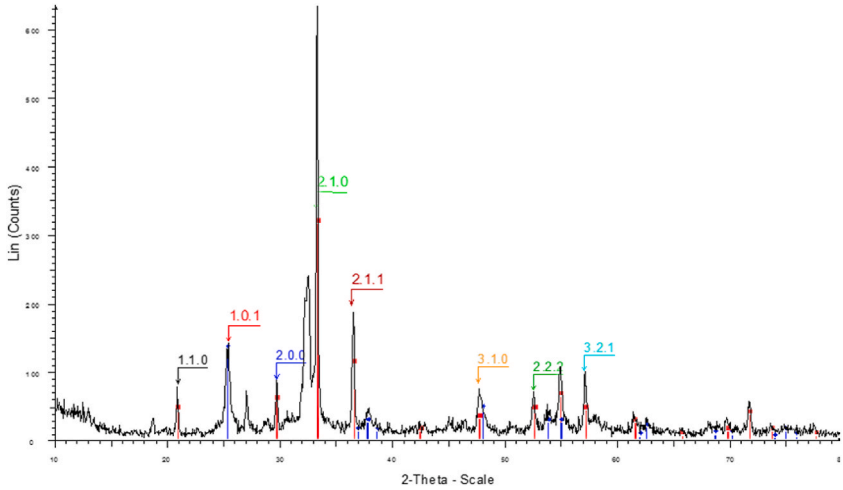

Fig. 3. XRD of Ag_3PO_4/TiO_2 heterogeneous catalyst.

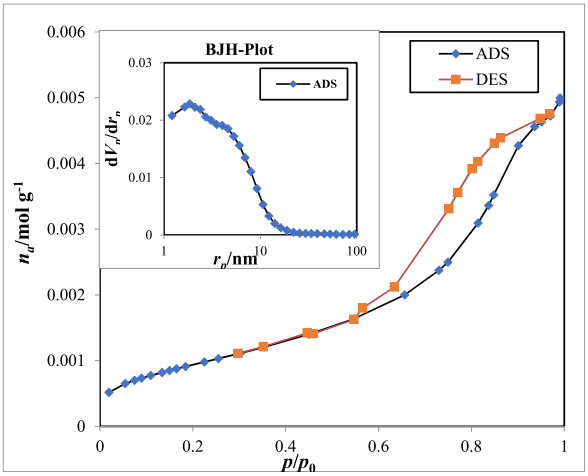

Fig. 4. Adsorption/desorption isotherm and BJH surface area of Ag_3PO_4/TiO_2 nanocatalyst.

3.2. Optimization of effective parameters on HA degradation

3.2.1. Effect of catalyst dose

Catalyst dosages of 0.1 to 0.3 g/L were investigated in the study of HA degradation. Fig. 5 shows that increasing the Ag_3PO_4/TiO_2

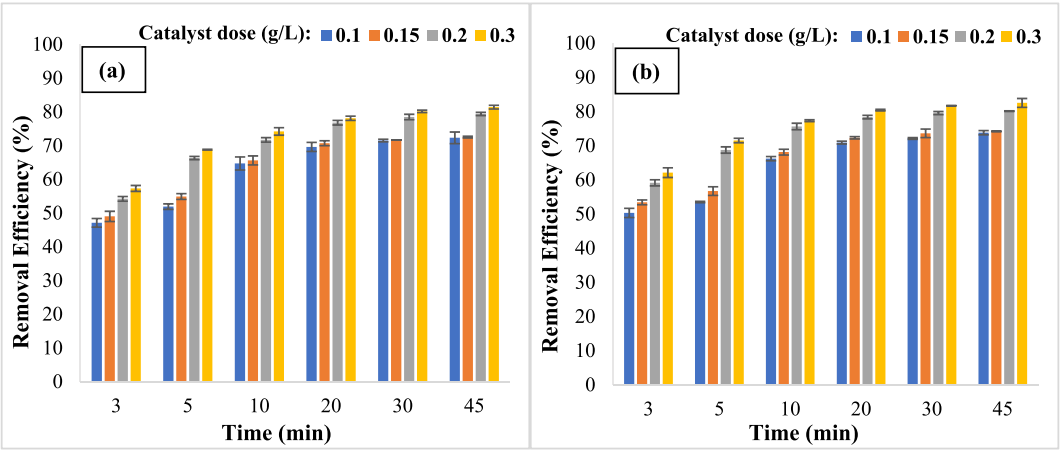

Fig. 5. Comparison of removal efficiency at different catalyst doses in presence of visible (a) and solar (b) light (HA concentration: 5 mg/L, pH: 7).

catalyst dosage from 0.1 to 0.3 g/L enhanced the removal effectiveness of HA from 69.6% to 78.1% for visible light and 70.9% to 80.4% for solar light in 20 min. The formation of additional hydroxyl radicals by the catalyst in the reaction medium may be the explanation for improving the effectiveness of HA degradation by raising the catalyst dosage. On the other hand, by raising the catalyst dosage from 0.2 to 0.3 g/L, the efficiency rises slightly from 76.8% to 78.1% in visible light and 78.4% to 80.4% in solar light, which might be attributed to a limitation of HA leaving in the reaction medium [43–45]. So, the 0.2 g/L of catalyst dose was considered an optimal catalyst dose. The presence of UV rays in sunlight explains how sunlight has a better efficacy of elimination than visible light. This beam excites the majority of electrons on the catalyst's surface and ultimately releases their energy, forcing water molecules to generate hydroxyl ($^{\bullet}OH$) and superoxide ($O_2^{\bullet}$) radicals, which then break down the HA molecules [46]. The findings of this study accord with those of Nasiri et al. which discovered that when the catalyst dosage is increased, the removal efficiency improves as well [47].

3.2.2. *Effect of HA initial concentration*

Concentration levels of 5, 10, and 25 mg/L were studied for the initial influence of HA on degrading effectiveness. Fig. 5 shows that when the concentration of HA increases from 5 to 25 mg/L, its degradation effectiveness declines from 76.8% to 62.5% for visible light (Fig. 6a) and from 78.4% to 63.3% for solar light (Fig. 6b) in 20 min. This was because raising the concentration of HA increased the formation of intermediates and by-products. However, while the quantity of $^{\bullet}OH$ and $O_2^{\bullet}$ generated in the reaction medium stayed unchanged, the significant inclination of by-products and intermediates to react with $^{\bullet}OH$ and $O_2^{\bullet}$ hindered additional decomposition of HA in the reaction medium, lowering its degradation effectiveness [41,48]. As a consequence, 5 mg/L of HA was shown to be the optimal initial concentration. Similar findings were achieved in research conducted by Khodadai et al. on the photocatalytic degradation of HA, and it was discovered that as the concentration of HA increases, its removal effectiveness decreases [49].

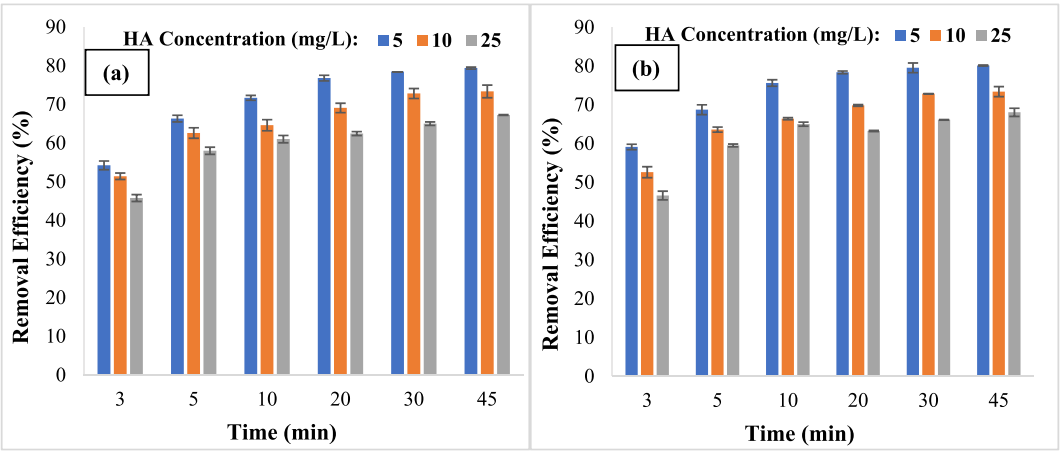

Fig. 6. Comparison of removal efficiency at different HA initial concentrations in presence of visible (a) and solar (b) light (Catalyst dose: 0.2 g/L, pH: 7).

3.2.3. Effect of pH on HA degradation

pH is a critical parameter that influences the solubility of HA, kinetics, radical generation, and catalyst surface characteristics. pHs 3, 7, and 11 were investigated to see how pH affected the removal effectiveness of HA. In this section, it was discovered that raising the pH from 3 to 11 reduces the removal effectiveness of visible light from 85.6% to 73.5% and solar light from 88.2% to 71.3% in 20 min (Fig. 7a and b). The insolubility and precipitation of HA in the reaction media, which is attributable to the nature of this organic matter, is one of the reasons for improving its removal effectiveness at acidic pH. When HA decomposes in the reaction medium, mineral compounds such as CO_2 are generated, and CO_2 is transformed to HCO_3^- in alkaline media, where it consumes active and energetic hydroxyl radicals. It generates $CO_3^{\bullet}$ radicals since it has decreased oxidation potential, lowering HA elimination efficiency (Eq. (2)) [46]. Furthermore, the surface charge of the catalyst turns negative at pHs over 6.7 and positive at pHs under 6.7, according to the catalyst's pH_{zpc} of 6.7 (Fig. 7c). Humic acid, on the other hand, has two $pKa_1 = 4$ and $pKa_2 = 8$, and it forms positively charged ions at pHs less than 4, zwitterion or neutral at pHs between 4 and 8, and negatively charged ions at pHs greater than 8, so at an optimum pH of 3, there are repulsive electrostatic forces, and HA is an organic molecule and hydrophobic interactions are dominant mechanism for near HA molecules to the catalyst surface, ultimately leading to degradation [50,51]. Similar results were achieved in Mohtar et al. investigation of the degradation of humic acid, confirming the findings of this study [52].

$$HCO_3^- + {}^{\bullet}OH \rightarrow CO_3^{\bullet} + H_2O \quad \text{(Eq. 2)}$$

3.3. Kinetic study of HA degradation

The *pseudo*-first-order kinetic (Eq. (3)) and Langmuir-Hinshelwood (Eq. (4)) models were used to examine HA degradation kinetics. The reactions that take place on the surface of reactants have different adsorption processes as well as rate equations that are essential for heterogeneous catalysis. One of the most frequent models for explaining heterogeneous catalytic processes is the Langmuir-Hinshelwood kinetic. The contaminant adsorption on catalyst active sites is studied in this model [53].

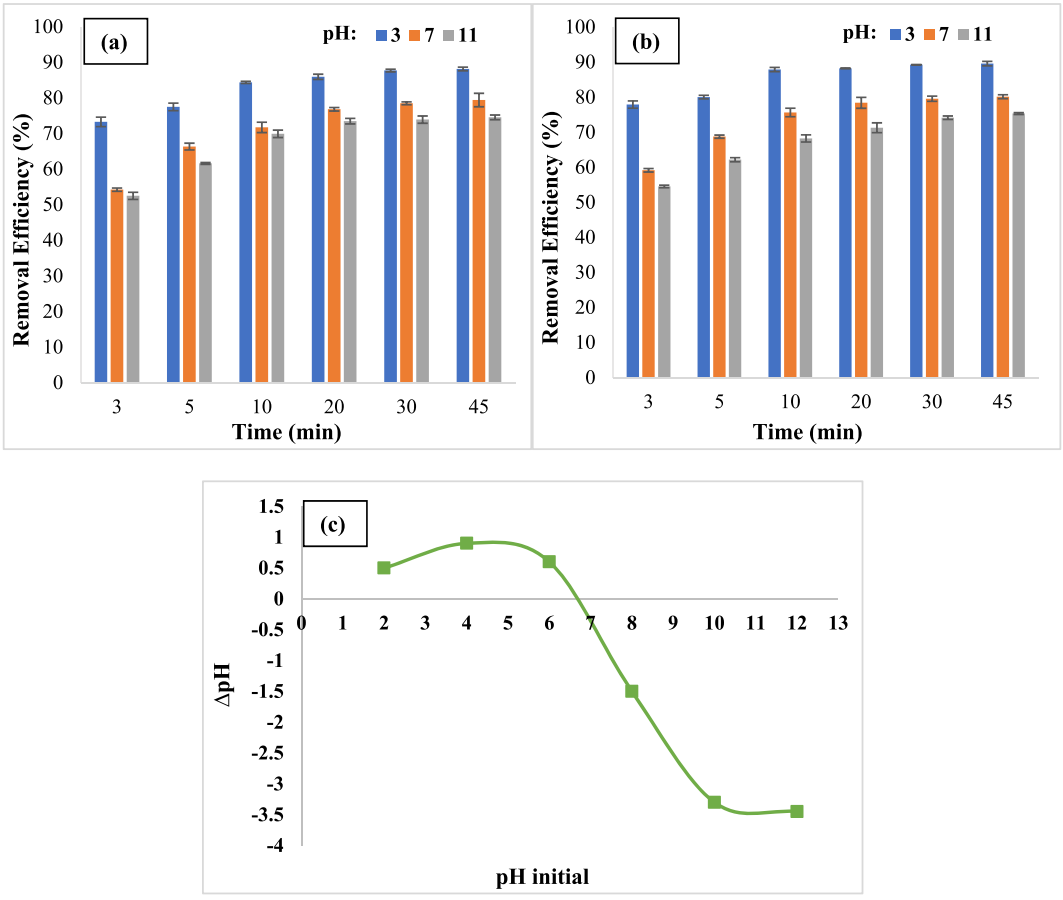

Fig. 7. Comparison of removal efficiency at different pHs in presence of visible (a), solar (b) light, and pH_{zpc} (c) (Catalyst dose: 0.2 g/L, HA concentration: 5 mg/L).

$$ln\frac{C_t}{C_0} = -K_{obs}t \quad \text{(Eq. 3)}$$

Where C_0 and C_t (mg/L) are the initial and after-contact HA concentrations, respectively, and K_{obs} is the reaction rate constant (min^{-1}).

$$\frac{1}{K_{obs}} = \frac{1}{K_C K_{L-H}} + \frac{C_0}{K_C} \quad \text{(Eq. 4)}$$

Where K_c represents the surface reaction rate constant (mg/L.min) and $K_{L\text{-}H}$ represents the adsorption equilibrium constant (L/mg). The value of K_{obs} was calculated for the various concentrations displayed in Table 1 by graphing $ln\ (C_t/C_0)$ vs time [45].

Then, utilizing the linear equation derived by graphing the curve K_{obs}^{-1} vs the initial concentration depicted in Fig. 8, the coefficients of K_c and $K_{L\text{-}H}$ were computed. The coefficients of K_c and $K_{L\text{-}H}$ were 0.729 mg/L.min and 0.036 L/mg, respectively, based on the result acquired from this curve. These findings also revealed that HA degrades according to *pseudo*-first-order and Langmuir-Hinshelwood kinetics. Research on humic acid decomposition was performed by Kamani et al. Humic acid decomposition follows pseudo-first-order and Langmuir-Hinshelwood kinetics, according to the study [54].

3.4. Investigation of process efficiency on real water

The impact of the Ag_3PO_4/TiO_2 catalyst process on HA degradation in real water was studied in this research. A sample of real water was obtained from a water treatment plant in Shiraz, Iran, according to parameters NO_3: 29.5 mg/L, total hardness: 462 mg/L, SO_4: 164 mg/L, Chloride: 81 mg/L, pH: 7.8, total dissolved solids (TDS): 665 mg/L, and Na: 54 mg/L. The removal effectiveness of HA from real water was 56% and 59.5% in presence of visible and solar light respectively, at the optimum conditions (pH 3, HA concentration 5 mg/L, and catalyst dosage 0.2 g/L) derived from the synthetic sample experiment, indicating the acceptable efficiency of this process in the treatment of real water. The reduced removal effectiveness of HA in real water may be attributed to the existence of impurities including cations, anions, TDS, as well as other impurities, which are removed as a consequence of the oxidation process; on the other hand, there could be inhibiting cations and anions in real water that serve as scavengers and diminish the activity of free radicals [55]. The findings of Acero et al. investigation of real water samples were similar to the findings of this study [56].

3.5. Degradation mechanism and stability of nanocatalyst

The heterogeneous catalyst structure between Ag_3PO_4 and TiO_2 can explain the increased photocatalytic activity of Ag_3PO_4/TiO_2 relative to ordinary TiO_2. The photocatalytic efficiency of TiO_2 is improved by coating Ag_3PO_4 on its surface, which enhances light absorption and enables electron-hole segregation according to their corresponding band orientations [57,58]. The border potentials of Ag_3PO_4's conduction band (CB) and valence band (VB) are +0.45 and + 2.9 eV, respectively, which are higher than TiO_2 (−0.5 and + 2.7 eV, respectively) [59–61]. Either Ag_3PO_4 and TiO_2 can be activated when exposed to light. Photon-generated holes in Ag_3PO_4's VB rapidly move to TiO_2, while photon-generated electrons move to Ag_3PO_4's CB. So, to the imposed electric field, photon-generated holes in the VB of Ag_3PO_4 might move to TiO_2 during light irradiation, whilst Ag_3PO_4 serves as a sensitizer absorbing light [45,62–64]. As a result, the electron-hole coupling mechanism is hindered, resulting in increased photoactivity of Ag_3PO_4/TiO_2. Under solar and visible light irradiation, the proposed mechanism of photocatalytic decomposition of HA over Ag_3PO_4/TiO_2. Photon-generated holes in Ag_3PO_4 particles easily move to the VB of TiO_2 when exposed to light. Since the VB value of TiO_2 (+2.7 eV) is more positive than the typical redox potential E° (OH/OH^-, 1.99 eV), the holes in the VB of TiO_2 may oxidize OH^- or H_2O to produce OH radicals (as demonstrated in Eqs. (3) and (4) [51,65]. Nevertheless, the CB of Ag_3PO_4 (+0.45 eV) is lower than the normal redox potential of E° (O_2/H_2O_2) (0.682 eV), implying that the electrons in the CB of Ag_3PO_4 can be transported to O_2 molecules adsorbed on the photocatalysts' surfaces and produce H_2O_2 [66]. As seen in Eqs. (5) and (6), H_2O_2 combines with electrons in a series to form active $^\bullet OH$ to some amount. As a result, strongly oxidative species such as $^\bullet OH$ and holes are generated, which react with the HA in aqueous media (Eq. (7)) [43,67].

$$h^+ + H_2O \rightarrow {}^\bullet OH + H^+ \quad \text{(Eq. 3)}$$

$$h^+ + OH^- \rightarrow {}^\bullet OH \quad \text{(Eq. 4)}$$

$$2e^- + O_2 + 2H^+ \rightarrow H_2O_2 \quad \text{(Eq. 5)}$$

$$e^- + H_2O_2 \rightarrow {}^\bullet OH + OH^- \quad \text{(Eq. 6)}$$

$$^\bullet OH,\ h^+ + HA \rightarrow CO_2 + H_2O + \ldots \quad \text{(Eq. 7)}$$

The nanocatalyst was filtered from the reaction media once the experiment was finished, and its structure was analyzed using SEM analysis (Fig. 9 a and b). According to the analysis's findings, the stability of the nanocatalysts was shown by the fact that their morphology was conserved once the reaction was over. The concentration of Ag (328.1 nm) and Ti (363.4 nm) were determined using an Atomic Absorption Spectrophotometer (AAS, CTA-3000) following the reaction in an aqueous solution to ascertain the chemical stability of Ag_3PO_4/TiO_2. The measurements made using this device's findings show that the concentration of Ag was 4.5 mg/L and Ti was below the AAS detection limit, indicating that this nanocatalyst has the necessary chemical stability [68,69].

To assess the main radicals in the humic acid degradation process, the radical scavenger's benzoquinone (BQ) and *tert*-butanol

Table 1
pseudo-first-order kinetic parameters of HA degradation.

C_0 (mg/L)	R^2	K_{obs}	Line Equation
5	0.837	52.356	y = −0.0191× - 1.6445
10	0.890	64.516	y = −0.0155× - 1.746
25	0.814	81.301	y = −0.0123× - 1.4367

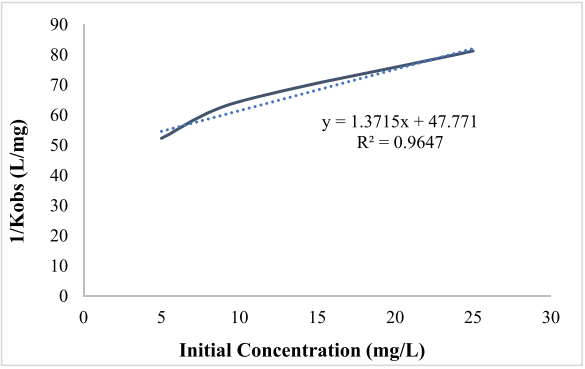

Fig. 8. Langmuir-Hinshelwood kinetic curve (Catalyst dose: 0.2 g/L, HA concentration: 5 mg/L, pH: 3, and time: 20 min).

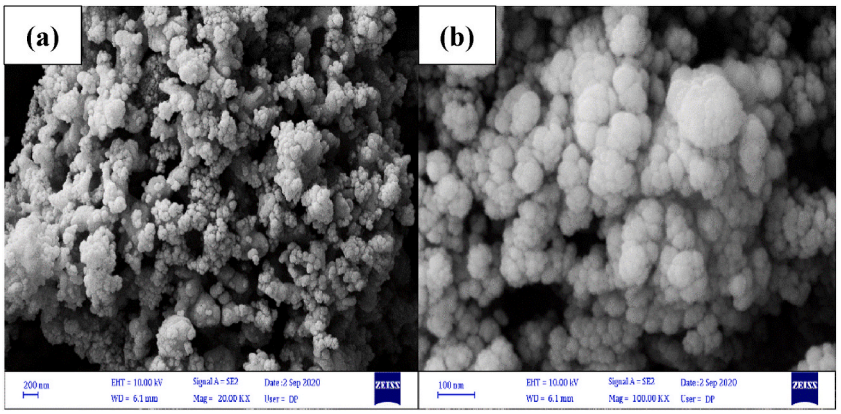

Fig. 9. SEM images after finishing process (a and b).

(TBA) were utilized for superoxide ($^{\bullet}O_2^-$) and hydroxyl radicals ($^{\bullet}OH$), respectively [70]. The elimination efficiency dropped from 88.2% to 61.5% when BQ was added to the reaction medium in the presence of solar light, and it dropped to 31.6% when TBA was added. This indicates that hydroxyl radicals were the dominant radicals in the degradation of humic acid.

Table 2
Comparison of the performance process VS other processes in HA degradation.

No.	Catalyst	Catalyst dose (g/L)	Initial Concentration (mg/L)	Time (min)	Removal Efficiency (%)	Ref.
1	$NiCo_2O_4$	0.2	10	120	90	[71]
2	$PAC/LaFeO_3/Cu$	0.72	5.33	36.2	95.5	[72]
3	$PE\text{-}TiO_2$	6.0	10	270	64.5	[73]
4	CeO_2/AC	0.5	50	30	75	[74]
5	TiO_2/Fe_2O_3	0.4	20	180	61.6	[75]
6	$CuO–Co_3O_4@AC$	0.5	100	60	88	[76]
7	Ag/ZnO	0.6	50	40	70	[77]
8	Ag_3PO_4/TiO_2	0.2	5	20	88.2	This study

3.6. Comparison with other catalysts to HA degradation

As indicated in Table 2, due to the experimental settings, the procedure examined in this study has a higher removal efficiency than in previous studies. Solar light has been utilized as a catalytic activator in all of the processes. Based on the findings of previous research, the amount of catalyst used in this study was reasonable given the high removal effectiveness and short contact time, and it was also higher cost-effective than some others.

4. Conclusion

A simple and effective approach was used to produce Ag_3PO_4/TiO_2 as a nano-heterogeneous catalyst. SEM, XRD, and EDS analyses were used to characterize the structure of this nano-heterogeneous catalyst. The particle size was 50–60 nm on the mean, according to SEM. The crystal structure of this catalyst was effectively retained, according to XRD measurements. Under optimum conditions, this catalyst removed humic acid from the aqueous medium with an efficiency of 88.2% and 85.9% in presence of solar light and visible light, respectively: catalyst dosage 0.2 g/L, starting concentration 5 mg/L, and pH 3. The decomposition of HA follows all these kinetics with coefficients of determination (R^2) of 0.837, 0.890, and 0.814 at concentrations of 5, 10, and 25 mg/L, respectively, according to the *pseudo*-first-order kinetic and Langmuir-Hinshelwood model. K_c and $K_{L\text{-}H}$ were also discovered to be 0.729 mg/L.min and 0.036 L mg, respectively. This catalyst's and process's effectiveness indicated that it may be used to remove other organic compounds.

Author contribution statement

Roya Morovati and Saeed Rajabi: Conceived and designed the experiments; performed the experiments; analyzed and interpreted the data; contributed reagents, materials, analysis tools or data; wrote the paper.

Mohammad Taghi Ghaneian and Mansooreh Dehghani: Conceived and designed the experiments; analyzed and interpreted the data; contributed reagents, materials, analysis tools or data; wrote the paper.

Data availability statement

Data will be made available on request.

Declaration of interest's statement

The authors declare no conflict of interest.

Acknowledgments

The present article was adopted from the proposal number 26063 and ethical cod IR.SUMS.SCHEANUT.REC.1401.101 approved by Shiraz University of Medical Sciences.

References

[1] Z. Liu, S.J.W.S. Zhou, Technology, Removal Of Humic Acid From Aqueous Solution Using Polyacrylamide/Chitosan Semi-IPN Hydrogel, 2018, pp. 16–26, 2017 (1).
[2] R. Morovati, et al., Degradation efficiency of humic acid in presence of hydrogen peroxide and ultrasonic from aqueous media, Desalination Water Treat. 281 (2023) 249–254.
[3] C.S. Uyguner, M.J.C.T. Bekbolet, Evaluation Of Humic Acid Photocatalytic Degradation By UV–Vis And Fluorescence Spectroscopy, 2005, pp. 267–274, 101 (3–4).
[4] E. Derakhshani, et al., A Systematic Review of Photocatalytic Degradation of Humic Acid in Aqueous Solution Using Nanoparticles, 2022.
[5] F. Yang, C. Tang, M.J.C.S.R. Antonietti, Natural And Artificial Humic Substances To Manage Minerals, Ions, Water, And Soil Microorganisms, 2021, pp. 6221–6239, 50(10).
[6] D. Ghernaout, et al., Removal of humic acids by continuous electromagnetic treatment followed by electrocoagulation in batch using aluminium electrodes 239 (1–3) (2009) 295–308.
[7] A. Barhoumi, et al., High-Rate Humic Acid Removal From Cellulose And Paper Industry Wastewater By Combining Electrocoagulation Process With Adsorption Onto Granular Activated Carbon, 2019, 111715, 140.
[8] S. Capasso, et al., Electrochemical Removal of Humic Acids from Water Using Aluminum Anode: Influence of Chloride Ion and Current Parameters, 2019, 2019.
[9] K. Rucka, A. Solipiwko-Pieścik, M.J.S.A.S. Wolska, Effectiveness Of Humic Substance Removal During The Coagulation Process, 2019, pp. 1–7, 1(6).
[10] V. Oskoei, et al., Removal Of Humic Acid From Aqueous Solution Using UV/Zno Nano-Photocatalysis And Adsorption, 2016, pp. 374–380, 213.
[11] A. Nasiri, et al., Adsorption of tetracycline using CuCoFe2O4@ Chitosan as a new and green magnetic nanohybrid adsorbent from aqueous solutions: isotherm, kinetic and thermodynamic study, Arab. J. Chem. 15 (8) (2022), 104014.
[12] A. Nasiri, et al., CuCoFe2O4@MC/AC as a new hybrid magnetic nanocomposite for Metronidazole removal from wastewater: bioassay and toxicity of effluent, Sep. Pur. Techn. (2022), 121366.
[13] M. Malakootian, et al., Investigation of nickel removal using poly(amidoamine) generation 4 dendrimer (PAMAM G4) from aqueous solutions, J. Eng. Res. 6 (2) (2018) 13–23.
[14] A. Nasiri, et al., CoFe2O4@methylcellulose synthesized as a new magnetic nanocomposite to tetracycline adsorption: modeling, analysis, and optimization by response surface methodology, J. Polym. Res. 28 (5) (2021).
[15] J.J.W.S. Fettig, Technology, Removal Of Humic Substances By Adsorption/Ion Exchange, 1999, pp. 173–182, 40(9).
[16] Y.-H. Cai, et al., Renewable energy powered membrane technology: Implications of adhesive interaction between membrane and organic matter on spontaneous osmotic backwash cleaning, 221, 2022, 118752.

[17] M. Rahmani Piani, et al., Removal of Humic Acids (HAs) in Drinking Water by Adsorption onto Polysulfone/Fe2O3 Mixed Matrix Membrane: Study kinetics and Isotherm Analysis, 2022, pp. 8–29, 16(1).
[18] H. Pezeshki, M. Hashemi, S. Rajabi, Removal of arsenic as a potentially toxic element from drinking water by filtration: a mini review of nanofiltration and reverse osmosis techniques, Heliyon 9 (3) (2023), e14246.
[19] G. Hasani, et al., Implementation of Pulsed Current Electro-Fenton Process for Humic Acid Removal from Aqueous Solutions: Optimization and Computational Analysis, 2021, 150929, 16.
[20] H. Hashemi, et al., Ozonation of secondary industrial effluent for beneficial reuse, Desalination Water Treat. 287 (2023) 96–102.
[21] M.T. Ghaneian, et al., Humic Acid Degradation By The Synthesized Flower-Like Ag/ZNO Nanostructure As An Efficient Photocatalyst, 2014, pp. 1–7, 12(1).
[22] A. Maleki, M. Seifi, N.J.J.o.C. Marzban, Evaluation of Sonocatalytic and Photocatalytic Processes Efficiency for Degradation of Humic Compounds Using Synthesized Transition-Metal-Doped ZnO Nanoparticles in Aqueous Solution, 2021, p. 2021.
[23] F.E. Titchou, et al., Removal Of Organic Pollutants From Wastewater By Advanced Oxidation Processes And Its Combination With Membrane Processes, 2021, 108631, 169.
[24] M.E. Taheri, et al., Fast photocatalytic degradation of bisphenol A by Ag3PO4/TiO2 composites under solar radiation, Catal. Today 280 (2017) 99–107.
[25] Z. Masood, et al., Application of Nanocatalysts in Advanced Oxidation Processes for Wastewater Purification: Challenges and Future Prospects, 2022, p. 741, 12 (7).
[26] R. Noroozi, et al., Catalytic Potential of CuFe2O4/GO For Activation Of Peroxymonosulfate In Metronidazole Degradation: Study Of Mechanisms, 2020, pp. 947–960, 18(2).
[27] S.B. Singh, P.K.J.J.E.C.E. Tandon, Catalysis: A Brief Review On Nano-Catalyst, 2014, pp. 106–115, 2(3).
[28] F.-M. Zhao, et al., Ag3PO4/TiO2 Composite For Efficient Photodegradation Of Organic Pollutants Under Visible Light, 2014, pp. 833–838, 317.
[29] S.B. Rawal, S. Do Sung, W.I.J.C.C. Lee, Novel Ag3PO4/TiO2 Composites For Efficient Decomposition Of Gaseous 2-Propanol Under Visible-Light Irradiation, 2012, pp. 131–135, 17.
[30] C. Tang, et al., Heterostructured Ag3PO4/TiO2 Nano-Sheet Film With High Efficiency For Photodegradation Of Methylene Blue, 2014, pp. 15447–15453, 40 (10).
[31] M. Khodadadi, et al., The Practical Utility Of The Synthesis FeNi3@ SiO2@ TiO2 Magnetic Nanoparticles As An Efficient Photocatalyst For The Humic Acid Degradation, 2020, 124723, 239.
[32] J.S. Salla, et al., Humic Acids Adsorption And Decomposition On Mn2O3 And A-Al2O3 Nanoparticles In Aqueous Suspensions In The Presence Of Ozone, 2020, 102780, 8(2).
[33] F.A. Tapouk, et al., Synthesis of PAC-LaFeO3-Cu Nanocomposites Via Sol-Gel Method For The Photo Catalytic Degradation Of Humic Acids Under Visible Light Irradiation, 2021, 105557, 9(4).
[34] H. Moein, et al., Efficiency Of Photocatalytic Degradation Of Humic Acid Using Magnetic Nanoparticles (Fe-Doped Tio2@ Fe3O4) In Aqueous Solutions, 2020, 9 (2).
[35] F.E. Bortot Coelho, et al., Photocatalytic Reduction Of Cr (VI) In The Presence Of Humic Acid Using Immobilized Ce–ZrO2 Under Visible Light, 2020, p. 779, 10 (4).
[36] M.T. Ghaneian, et al., Photocatalytic Degradation of Humic Acid by Ag/ZnO Nanoparticles under UVC Irradiation from Aqueous Solutions, 2014.
[37] X. Yao, et al., Degradation Of Humic Acid Using Hydrogen Peroxide Activated By CuO-Co3O4@ AC Under Microwave Irradiation, 2017, pp. 783–791, 330.
[38] M. Khodadadi, et al., FeNi3@ SiO2 Magnetic Nanocomposite As A Highly Efficient Fenton-Like Catalyst For Humic Acid Adsorption And Degradation In Neutral Environments, 2018, pp. 258–267, 118.
[39] W. Yao, et al., Synthesis and characterization of high efficiency and stable Ag 3 PO 4/TiO 2 visible light photocatalyst for the degradation of methylene blue and rhodamine B solutions, J. Mater. Chem. 22 (9) (2012) 4050–4055.
[40] A. Nasiri, S. Rajabi, M. Hashemi, CoFe2O4@ methylcellulose/AC as a new, green, and eco-friendly nano-magnetic adsorbent for removal of reactive red 198 from aqueous solution, Arab. J. Chem. (2022), 103745.
[41] S. Rajabi, A. Nasiri, M. Hashemi, Enhanced activation of persulfate by CuCoFe2O4@ MC/AC as a novel nanomagnetic heterogeneous catalyst with ultrasonic for metronidazole degradation, Chemosphere 286 (3) (2022), 131872.
[42] M. Malakootian, A. Nasiri, H. Mahdizadeh, Preparation of CoFe2O4/activated carbon@ chitosan as a new magnetic nanobiocomposite for adsorption of ciprofloxacin in aqueous solutions, Water Sci. Technol. 78 (10) (2018) 2158–2170.
[43] H. Mahdizadeh, et al., Hybrid UV/COP advanced oxidation process using ZnO as a catalyst immobilized on a stone surface for degradation of acid red 18 dye, MethodsX 7 (2020).
[44] A. Nasiri, et al., A microwave assisted method to synthesize nanoCoFe2O4@methyl cellulose as a novel metal-organic framework for antibiotic degradation, MethodsX 6 (2019) 1557–1563.
[45] F. Tamaddon, et al., Microwave-assisted preparation of ZnFe2O4@methyl cellulose as a new nano-biomagnetic photocatalyst for photodegradation of metronidazole, Int. J. Biol. Macromol. 154 (2020) 1036–1049.
[46] H. Gong, et al., Solar photocatalytic degradation of ibuprofen with a magnetic catalyst: effects of parameters, efficiency in effluent, mechanism and toxicity evolution, Environ. Pollut. 276 (2021), 116691.
[47] A. Nasiri, et al., CoFe2O4@Methylcelloluse as a new magnetic nano biocomposite for sonocatalytic degradation of reactive blue 19, J. Polym. Environ. 29 (8) (2021) 2660–2675.
[48] M. Forouzesh, A. Ebadi, A. Aghaeinejad-Meybodi, Degradation of metronidazole antibiotic in aqueous medium using activated carbon as a persulfate activator, Sep. Purif. Technol. 210 (2019) 145–151.
[49] M. Khodadadi, et al., The practical utility of the synthesis FeNi3@ SiO2@ TiO2 magnetic nanoparticles as an efficient photocatalyst for the humic acid degradation, Chemosphere 239 (2020), 124723.
[50] N. Aarab, et al., Removal of an emerging pharmaceutical pollutant (metronidazole) using PPY-PANi copolymer: kinetics, equilibrium and DFT identification of adsorption mechanism, Groundwat. Sustain. Develop. 11 (2020), 100416.
[51] M. Malakootian, et al., Synthesis and stabilization of ZnO nanoparticles on a glass plate to study the removal efficiency of acid red 18 by hybrid advanced oxidation process (Ultraviolet/ZnO/ultrasonic), Desalination Water Treat. 170 (2019) 325–336.
[52] S.S. Mohtar, et al., Photocatalytic degradation of humic acid using a novel visible-light active α-Fe2O3/NiS2 composite photocatalyst, J. Environ. Chem. Eng. 9 (4) (2021), 105682.
[53] J. Alvarez-Ramirez, et al., Some remarks on the Langmuir–Hinshelwood kinetics, J. Math. Chem. 54 (2) (2016) 375–392.
[54] H. Kamani, et al., Catalytic degradation of humic acid using Fe–doped TiO2-ultrasound hybrid system from aqueous solution, Int. J. Environ. Anal. Chem. (2021) 1–15.
[55] E.S. Elmolla, M. Chaudhuri, Photocatalytic degradation of amoxicillin, ampicillin and cloxacillin antibiotics in aqueous solution using UV/TiO2 and UV/H2O2/TiO2 photocatalysis, Desalination 252 (1–3) (2010) 46–52.
[56] J.L. Acero, et al., Degradation of neonicotinoids by UV irradiation: kinetics and effect of real water constituents, Sep. Pur. Techn. 211 (2019) 218–226.
[57] P. Zhu, et al., Nd2Sn2O7/Bi2Sn2O7/Ag3PO4 double Z-type heterojunction for antibiotic photodegradation under visible light irradiation: mechanism, optimization and pathways, Sep. Pur. Techn. 300 (2022), 121897.
[58] P. Zhu, et al., Visible light response photocatalytic performance of Z-scheme Ag3PO4/GO/UiO–66–NH2 photocatalysts for the levofloxacin hydrochloride, Langmuir 37 (45) (2021) 13309–13321.
[59] B. Liu, et al., Low temperature fabrication of V-doped TiO2 nanoparticles, structure and photocatalytic studies, J. Hazard Mater. 169 (1–3) (2009) 1112–1118.
[60] M.A. Barakat, R. Kumar, Photocatalytic activity enhancement of titanium dioxide nanoparticles, in: Photocatalytic Activity Enhancement of Titanium Dioxide Nanoparticles, Springer, 2016, pp. 1–29.

[61] M. Hu, et al., Construction of Ag3PO4/TiO2/C with pn heterojunction using Shiff base-Ti complex as precursor: preparation, performance and mechanism, Powder Technol. 393 (2021) 597–609.
[62] Z. Yi, et al., An orthophosphate semiconductor with photooxidation properties under visible-light irradiation, Nat. Mater. 9 (7) (2010) 559–564.
[63] M. Malakootian, et al., Decoloration of textile Acid Red 18 dye by hybrid UV/COP advanced oxidation process using ZnO as a catalyst immobilized on a stone surface, Desalination Water Treat. 182 (2020) 385–394.
[64] P. Zhu, et al., Construction and mechanism of a highly efficient and stable Z-scheme Ag 3 PO 4/reduced graphene oxide/Bi 2 MoO 6 visible-light photocatalyst, Catal. Sci. Technol. 8 (15) (2018) 3818–3832.
[65] X. Fu, et al., V2O5/Al2O3 composite photocatalyst: preparation, characterization, and the role of Al2O3, Chem. Eng. J. 180 (2012) 170–177.
[66] M. Malakootian, et al., Experimental data on the removal of phenol by electro-H2O2 in presence of UV with response surface methodology, MethodsX 6 (2019) 1188–1193.
[67] M. Antoniadou, P. Lianos, Production of electricity by photoelectrochemical oxidation of ethanol in a PhotoFuelCell, Appl. Catal. B Environ. 99 (1–2) (2010) 307–313.
[68] M. Resano, M. Flórez, E. García-Ruiz, High-resolution continuum source atomic absorption spectrometry for the simultaneous or sequential monitoring of multiple lines. A critical review of current possibilities, Spectrochim. Acta B Atom Spectrosc. 88 (2013) 85–97.
[69] F. Kurşun, B. Dağci, C. Özcan, Determination of titanium in zinc ash by FAAS after digested using ultrasound-assisted extraction, Kırklareli Üniversitesi Mühendislik ve Fen Bilimleri Dergisi 7 (1) (2021) 147–154.
[70] X. Wang, et al., Degradation of microcystin-LR by highly efficient AgBr/Ag3PO4/TiO2 heterojunction photocatalyst under simulated solar light irradiation, Appl. Surf. Sci. 325 (2015) 1–12.
[71] X. Tian, et al., Controlled synthesis of dandelion-like NiCo2O4 microspheres and their catalytic performance for peroxymonosulfate activation in humic acid degradation, Chem. Eng. J. 331 (2018) 144–151.
[72] F.A. Tapouk, et al., Synthesis of PAC-LaFeO3-Cu nanocomposites via sol-gel method for the photo catalytic degradation of humic acids under visible light irradiation, J. Environ. Chem. Eng. 9 (4) (2021), 105557.
[73] S. Valencia, J. Marín, G. Restrepo, Photocatalytic degradation of humic acids with titanium dioxide embedded into polyethylene pellets to enhance the postrecovery of catalyst, Environ. Eng. Sci. 35 (3) (2018) 185–193.
[74] H. Qin, et al., Kinetics and mechanism of humic acids degradation by ozone in the presence of CeO2/AC, Ozone: Sci. Eng. 37 (4) (2015) 371–378.
[75] S. Qiao, et al., Photocatalytic oxidation technology for humic acid removal using a nano-structured TiO2/Fe2O3 catalyst, Water Sci. Technol. 47 (1) (2003) 211–217.
[76] X. Yao, et al., Degradation of humic acid using hydrogen peroxide activated by CuO-Co3O4@ AC under microwave irradiation, Chem. Eng. J. 330 (2017) 783–791.
[77] M.T. Ghaneian, et al., Humic acid degradation by the synthesized flower-like Ag/ZnO nanostructure as an efficient photocatalyst, J. Environ. Heal. Sci. Eng. 12 (1) (2014) 1–7.